Article

Cell Reports

Structure-Based Design of Prefusion-Stabilized Filovirus Glycoprotein Trimers

Graphical Abstract

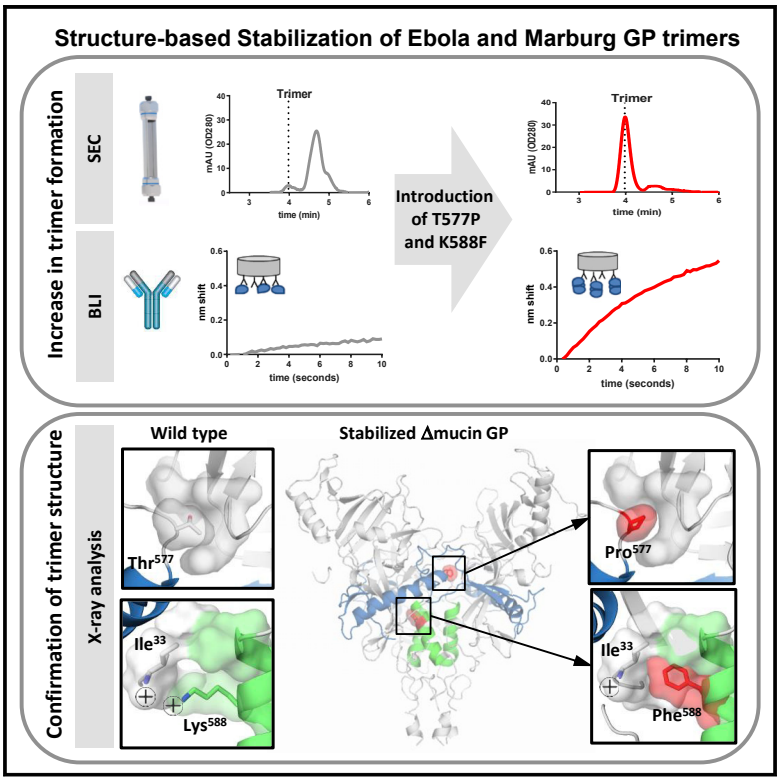

Highlights

- Filovirus GP expression increases by stabilizing mutations in hinge loop and base helix
- Charged lysine in base helix and GP1 N terminus are trapped in metastable conformation
- Crystal structure of stabilized Makona Δmucin GP confirms successful stabilization
- These findings may be useful for understanding fusion mechanisms and vaccine design

Authors

Lucy Rutten, Morgan S.A. Gilman, Sven Blokland, Jarek Juraszek, Jason S. McLellan, Johannes P.M. Langedijk

Correspondence

jmclellan@austin.utexas.edu (J.S.M.), hlangedi@its.jnj.com (J.P.M.L.)

In Brief

Rutten et al. describe structure-based stabilization of soluble filovirus GP trimers to obtain high yields of trimers. The crystal structure of a stabilized Makona Δmucin GP shows how the introduced substitutions stabilize the trimer and that the N terminus of GP1 plays a crucial role in refolding.

Rutten et al., 2020, Cell Reports *30*, 4540–4550
March 31, 2020
https://doi.org/10.1016/j.celrep.2020.03.025

CellPress

OPEN ACCESS
CellPress

Cell Reports
Article

Structure-Based Design of Prefusion-Stabilized Filovirus Glycoprotein Trimers

Lucy Rutten,[1,3] Morgan S.A. Gilman,[2,3] Sven Blokland,[1] Jarek Juraszek,[1] Jason S. McLellan,[2,*] and Johannes P.M. Langedijk[1,4,*]

[1]Janssen Vaccines & Prevention, Archimedesweg 4–6, Leiden 2333 CN, the Netherlands
[2]Department of Molecular Biosciences, The University of Texas at Austin, Austin, TX 78712, USA
[3]These authors contributed equally
[4]Lead Contact
*Correspondence: jmclellan@austin.utexas.edu (J.S.M.), hlangedi@its.jnj.com (J.P.M.L.)
https://doi.org/10.1016/j.celrep.2020.03.025

SUMMARY

Ebola virus causes severe hemorrhagic fever, often leading to death in humans. The trimeric fusion glycoprotein (GP) is the sole target for neutralizing antibodies and is the major focus of vaccine development. Soluble GP ectodomains are unstable and mostly monomeric when not fused to a heterologous trimerization domain. Here, we report structure-based designs of Ebola and Marburg GP trimers based on a stabilizing mutation in the hinge loop in refolding region 1 and substitution of a partially buried charge at the interface of the GP1 and GP2 subunits. The combined substitutions (T577P and K588F) substantially increased trimer expression for Ebola GP proteins. We determined the crystal structure of stabilized GP from the Makona *Zaire ebolavirus* strain without a trimerization domain or complexed ligand. The structure reveals that the stabilized GP adopts the same trimeric prefusion conformation, provides insight into triggering of GP conformational changes, and should inform future filovirus vaccine development.

INTRODUCTION

Filovirus infections are characterized by high fatality rates, with repeated outbreaks occurring in West Africa. Most are local outbreaks, but in 2014, an epidemic caused by the *Zaire ebolavirus* spread throughout West Africa, resulting in more than 11,000 deaths (World Health Organization, 2020a). The current epidemic in the Democratic Republic of Congo is the second largest, with more than 2,264 deaths, to date and has been declared a public health emergency of international concern (World Health Organization, 2020b).

The *Filoviridae* family comprises six genera, with members of the genus *Marburgvirus* (one species: *Marburg marburgvirus*) and the genus *Ebolavirus* (six species: *Bombali ebolavirus*, *Bundibugyo ebolavirus*, *Reston ebolavirus*, *Sudan ebolavirus*, *Tai Forest ebolavirus*, and *Zaire ebolavirus*) being the most significant threats to human health (Kuhn et al., 2019) (International Committee on Taxonomy of Viruses, 2019). Filovirus glycoprotein (GP) is a class I fusion protein that consists of two disulfide-linked subunits, GP1 and GP2, that trimerize to form the active molecule on the virion surface. GP1 consists of a core, a glycan cap, and a mucin-like domain. GP2 is anchored to the membrane and contains the membrane-fusion domains. Like other viral fusion proteins, filovirus GP is a dynamic machine that drives membrane fusion by irreversibly refolding from a metastable prefusion conformation to a stable postfusion conformation. In the case of Ebola virus, the unusually complex entry requirements are (1) binding to a cell-surface receptor (TIM-1, Axl, heparan sulfate, and DC-SIGN) (Alvarez et al., 2002; Brindley et al., 2011; Jemielity et al., 2013; Kondratowicz et al., 2011; Shimojima et al., 2007; Simmons et al., 2003; Takada et al., 2000); (2) macropinocytosis (Mulherkar et al., 2011; Nanbo et al., 2010; Saeed et al., 2010); (3) cleavage of GP at low pH by cathepsins (Chandran et al., 2005; Schornberg et al., 2006); (4) binding to loop C of Niemann-Pick C1 cholesterol transporter in the endosome (Carette et al., 2011; Côté et al., 2011; Miller et al., 2012; Wang et al., 2016); and most likely, (5) a final trigger that drives GP to undergo the conformational changes required for membrane fusion (Fénéant et al., 2019; Wang et al., 2016).

For many class I fusion proteins, stabilizing substitutions have been described for vaccine applications or to facilitate structural analysis (Binley et al., 2000; Fels et al., 2019; Hastie et al., 2017; Krarup et al., 2015; McLellan et al., 2013; Pallesen et al., 2017; Rutten et al., 2018; Sanders et al., 2002). However, no stabilizing substitutions have been described for soluble filovirus GP trimer. Moreover, GP structures that have been obtained previously have included a trimerization domain, complexed antibodies, or a non-native N terminus (Bale et al., 2012; Bornholdt et al., 2016; Dias et al., 2011; Janus et al., 2018; Lee et al., 2008; Murin et al., 2018; Pallesen et al., 2016; Wang et al., 2016; West et al., 2018). Because GP ectodomains form a mixture of species when expressed in HEK293T cells (Figure S8 in Lee et al., 2008), we sought to stabilize the trimeric, prefusion conformation of GP. We mutated elements in refolding region 1 (RR1, from 502 to 584) of GP2 and at the interface between GP1 and GP2 to obtain high yields of near-native soluble filovirus prefusion GP trimers with a native N terminus and without a heterologous trimerization domain. The trimers described in this study allowed structure

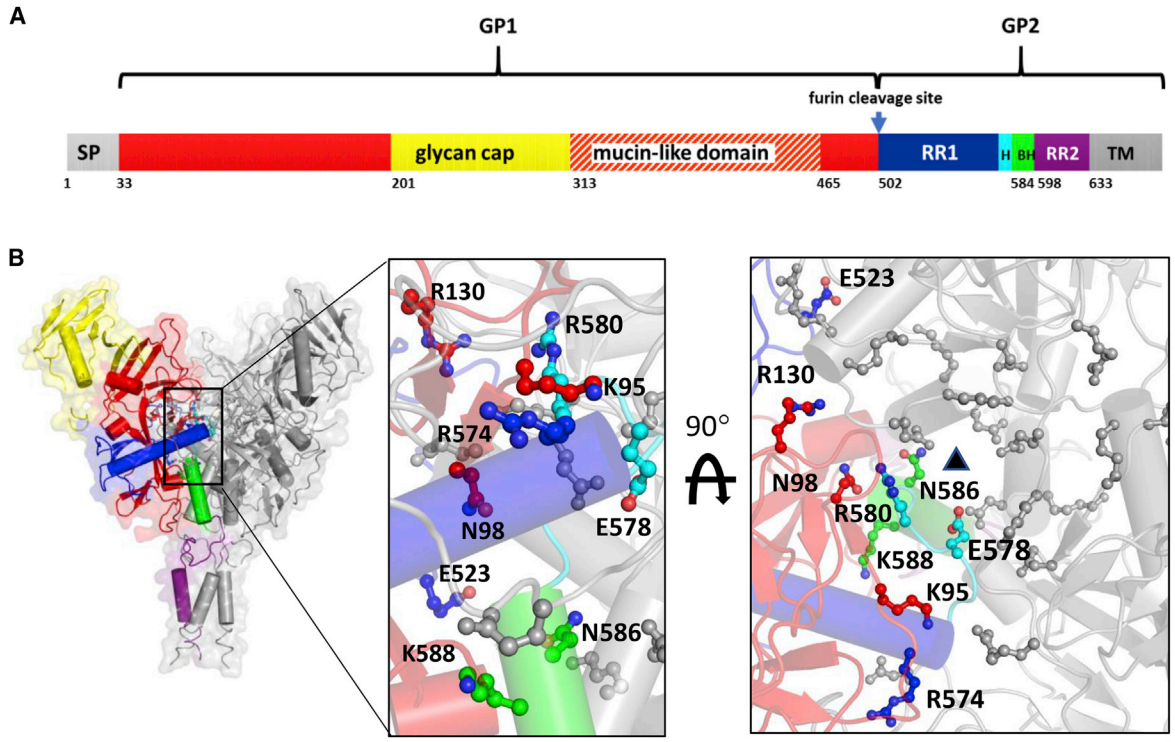

Figure 1. Structure-Based Design of Stabilizing Mutations

(A) Schematic structure of filovirus GP showing the GP1 head domain (red, yellow) that includes the mucin-like domain (dashed red/white) and the glycan cap (yellow), GP2 that includes RR1 (with the hinge region in cyan), the base helix (BH, between RR1 and RR2) in green, refolding region 2 (RR2, in purple), and the transmembrane domain (TM, in gray).

(B) Cartoon of the 5JQ3 crystal structure used for the structure-based design. Coloring is as in (A). Amino acid residues shown as a ball-and-stick model were selected for mutagenesis.

determination of an unliganded Ebola GP ectodomain with a native N terminus, revealing the importance of the N terminus in the stability of the prefusion GP trimer. The stabilized soluble trimers described here may have applications as superior subunit-based antigens in vaccines or immune assays or as bait for isolation of monoclonal antibodies (mAbs) against filovirus GPs.

RESULTS

Structure-Based Design of Stabilized GP Trimers

The ectodomains of wild-type *Zaire ebolavirus* GPs from the Yambuku-Mayinga and Makona strains were expressed with or without their mucin-like domains and without an additional C-terminal trimerization domain. Only a small fraction of the total produced protein formed trimers, as judged by analytical size-exclusion chromatography (SEC) or native polyacrylamide gel electrophoresis (PAGE), whereas most of the protein formed dimers and monomers (Figure S1). To increase the trimer yields, we set out to increase the stability of the protein using a structure-based design. Although class I fusion proteins like HIV-1 Env, respiratory syncytial virus (RSV) F, influenza hemagglutinin (HA), and Ebola/Marburg GP have very low sequence conservation, they share structural features in their fusion machinery. Because class I fusion proteins need to transform from a prefusion conformation to a highly stable postfusion conformation, the proteins harbor several regions of instability. The C-terminal end of RR1 just before the base helix is the so-called hinge region (Figure 1) that needs to transform from a loop to a coiled-coil structure. Mutations to proline in the hinge loop of RR1 have been successful in arresting this transition and stabilizing other class I fusion proteins (Battles et al., 2017; Hastie et al., 2017; Krarup et al., 2015; Pallesen et al., 2017; Sanders et al., 2002). Other approaches that proved successful were the neutralization of charged repulsions or the substitution of buried charged and polar residues in subdomain interfaces (Krarup et al., 2015; Rutten et al., 2018). Both approaches were explored for Ebola GP.

Hinge Loop Stabilization

Plasmids encoding soluble Makona GP variants with proline substitutions in the hinge loop at positions 575, 576, 577, 579, and 581 were transfected in Expi293F cells. Cell culture supernatants were tested for trimer formation using native PAGE (Figure 2A). L579P and T577P increased the trimer yield of Makona GP, and the double mutation (T577P/L579P) further increased the yield, as shown by analytical SEC of cell culture supernatants (Figure 2B). T577P increased the melting temperature in which 50% of the protein was unfolded (T_{m50}) by ~2.5°C, whereas

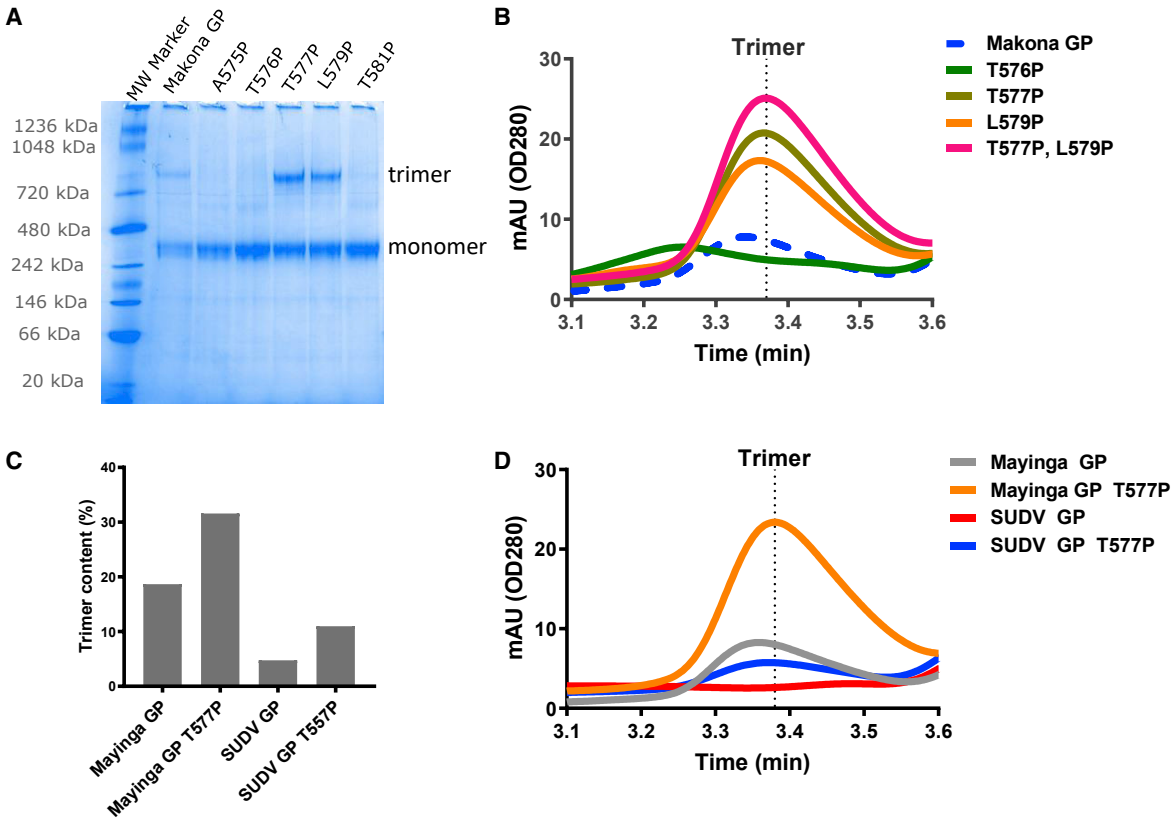

Figure 2. Increased Trimer Yield by Prolines in RR1 Hinge Loop in Ebola GP

(A and B) Native PAGE (A) and analytical SEC profile (B) of variants with single and double proline mutations in the hinge loop of Makona GP. Analysis was performed on crude cell culture supernatants.

(C) Quantification of expression levels of Mayinga and Sudan (Gulu) (SUDV) GP trimers observed in native PAGE gel (data not shown) with and without the T577P mutation. The y axis shows the trimer content, based on the intensity of the trimer band and monomer bands, as a percentage of trimer content.

(D) Analytical SEC profiles of Mayinga and SUDV GP with and without T577P. Analysis was performed on crude cell culture supernatants.

L579P did not increase the T_{m50} of Makona GP (Figure S2). Introduction of the T577P substitution in Makona GP that lacked the mucin-like region (Δmucin GP) showed a ~10-fold increase in trimer yield (Figure S3). The hinge loop stabilization was also tested for Mayinga and Sudan (Gulu) (SUDV) GP. Excluding the mucin-like domain, Makona and Mayinga GPs are ~97% identical and Makona and Sudan (Gulu) GPs are ~70% identical. Both Mayinga and Sudan (Gulu) GPs showed substantially increased trimer yields when T577P was introduced (Figures 2C and 2D), demonstrating the general applicability of the hinge loop stabilization approach.

Stabilization by Optimization of Domain Interfaces

Subdomains in viral fusion proteins need to refold and move relative to each other; therefore, such proteins do not contain the hydrophobic core of a typical protein. We identified nine charged and polar residues that are buried to different extents in the inter-protomer interface or the interface between GP1 and GP2. All of these residues are clustered in the charged center of the structure, close to the hinge loop (Figure 1B). These amino acids were substituted with hydrophobic residues in Makona Δmucin GP. Supernatants of cell cultures transfected with the GP variants with single or double substitutions were analyzed by native PAGE (Figure S4A). The variants that showed increased trimer formation were further analyzed by analytical SEC (Figures 3A and S4B). The K588W and K588F substitutions showed a substantial increase in trimer expression, and few monomers were detected for the K588F variant (Figure 3A). To investigate the nature of the stabilizing effect of K588F, other substitutions were evaluated at position 588 for Mayinga GP and Mayinga Δmucin GP. Most hydrophobic residues at position 588 increased trimer yield, as shown by analytical SEC (Figures 3B and 3D) or binding to the trimer-specific antibody mAb100 (Figures 3C and 3E). Although the footprint of mAb100 is distributed over two monomers at the trimer interface, it is not known whether mAb100 can also bind to monomeric GP with reduced affinity. However, the association rate of mAb100 with the GP variants, as measured by bio-layer interferometry (BLI), correlated with the amounts of trimer measured using analytical SEC (Figure S5A). The association rate with samples that contain more monomeric GP is low, but at saturation after 300 s, the nanometer shift no longer correlates with the trimer content but with the total amount of GP trimer and monomer in the sample. This indicates that mAb100 may also bind to monomers and

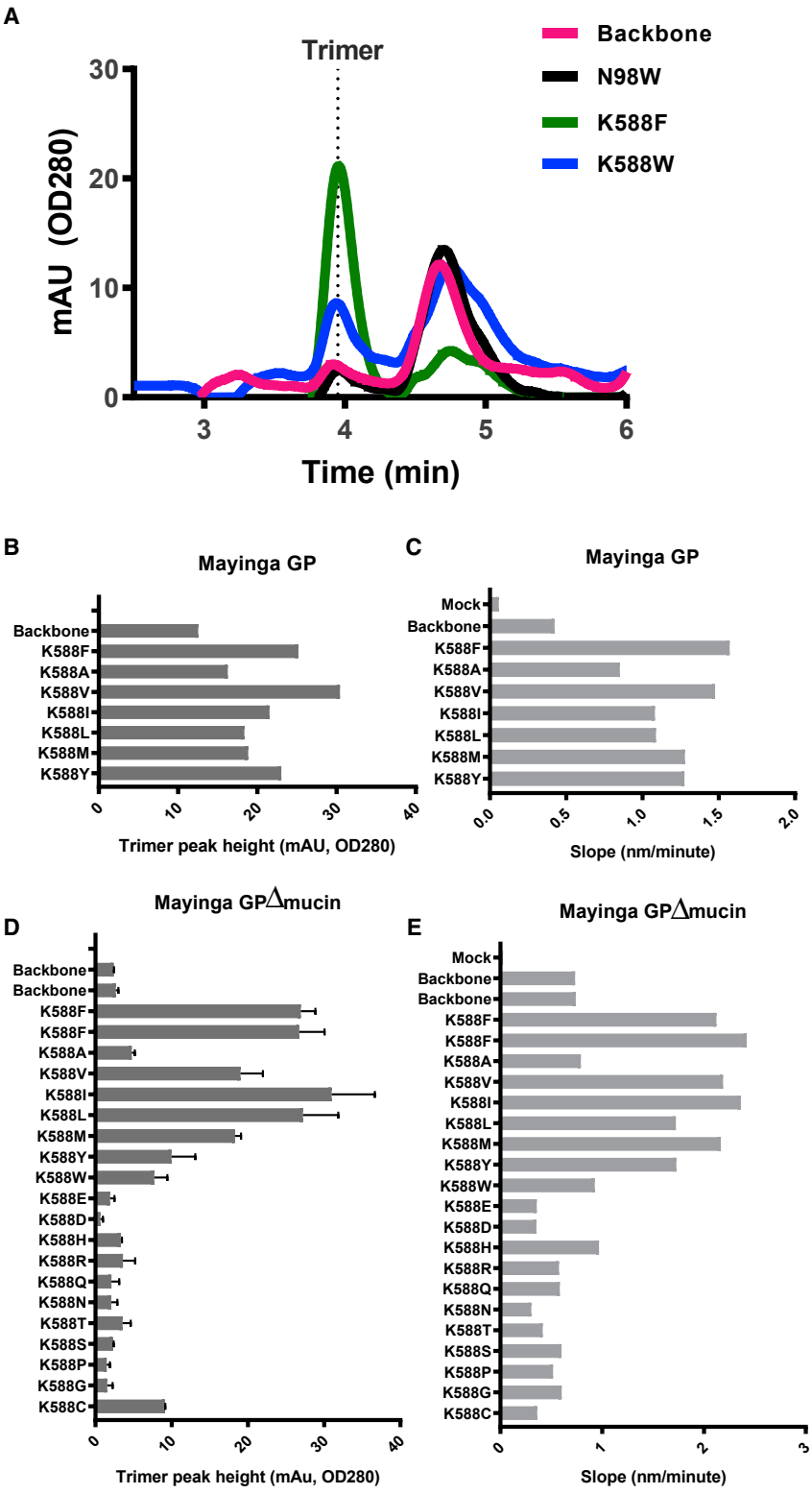

Figure 3. Substitutions at Position 588 Increase Trimer Expression

(A) Analytical SEC profile of the variants with substitutions that increased the trimer content in the Makona Δmucin GP T577P/T42A backbone. The trimer peak is labeled ~4 min.

(B) Expression levels of Mayinga GP trimers based on analytical SEC trimer peak heights for variants with hydrophobic substitutions of Lys588.

(C) BLI binding rates after 10 s of binding of mAb100.

(D) Expression levels of Mayinga Δmucin GP trimers based on analytical SEC trimer peak heights for variants with all possible natural substitutions of Lys588. Data are represented as mean ± SEM.

(E) BLI binding rates after 10 s of binding of mAb100. Analysis was performed on crude cell culture supernatant.

See also Figures S4 and S5 and Table S1.

could indicate that mAb100 is able to induce trimer formation. Surprisingly, although the K588F mutation increases trimer content, it slightly decreased the T_{m50} by ~1.2°C. (Figure S2B).

Combination of Substitutions and General Application of Approach for Other Filovirus GPs

The combined T577P and K588F substitutions were evaluated for their impact on Mayinga, Makona, and SUDV GP trimer stabilization with and without the mucin-like domain. The Mayinga GP with an N-terminal HA tag and T42A/T230V substitutions (Lee et al., 2008) was included as a control. Trimer content was determined using analytical SEC, and association phase analysis with mAb100 was determined using BLI. The T577P and K588F substitutions increased the trimer yield, and the combination of both substitutions resulted in the highest trimer yields (Figures 4A, 4B, and S5B) and increased the fraction of trimeric GP in the HA-tagged T42A/T230V variant (Lee et al., 2008) (Figure 4A, gray curve in lower left panel). The substitutions at positions 578 (equivalent to 577 in Ebola GP) and 589 (equivalent to 588 in Ebola GP) were also introduced in Marburg GP, which only has ~32% sequence identity with Ebola GP. Although the T578P substitution did not show a stabilizing effect on the Marburg Δmucin GP trimer (data not shown), the H589F and H589I substitutions increased the levels of the Marburg Δmucin GP trimers compared with the wild-type ectodomain. The wild-type Marburg Δmucin predominantly formed high-molecular-weight aggregates, as shown by analytical SEC and native PAGE (Figures 4C and S5C). Although the retention time of the Marburg Δmucin GP trimers in analytical SEC is shorter than that of the Ebola Δmucin GP trimers, they have similar average molecular weights according to multi-angle light scattering (MALS) (214.0 and ~213.7 kDa for the H589I and H589F Marburg Δmucin GP variants, respectively) (Figure 4D; Table S1). When only the protein fraction molecular weights (MWs) are calculated, without glycosylation, the MWs are close to the theoretical MW based on the sequence (Table S1). From this, we conclude that the elution peak at 3.6 min contains Marburg Δmucin GP trimers.

Crystal Structure of Makona GP with T577P and K588F Mutations

To identify the effect of the stabilizing mutations on the conformation of trimeric prefusion GP, we determined the X-ray crystal structure of apo T577P/K588F Makona GP at pH 5.2 For these studies, the mucin-like region was deleted to facilitate crystallization (Figure 5A). The 3.5 Å resolution structure (see Table S2 for crystallographic statistics) revealed that stabilized GP is similar to the previously determined Mayinga GP structure (PDB: 5JQ3), with an root-mean-square deviation (RMSD) of 1.87 Å for 353 Cα atoms. Although small differences in the conformation of the fusion loop were evident, the native conformation of the hinge loop and the base helix was preserved (Figures 5B and 5C). Thus, the stabilizing mutations did not disrupt the overall conformation of the trimeric prefusion GP protein. Pro577 is located at the inter-protomer interface (Figure 5B). The proline likely has a stabilizing effect because of prevention of α-helical formation and thus the transition from prefusion to postfusion conformation, but it could also stabilize the packing between two protomers. The proline makes more favorable van der Waals interactions with the neighboring protomer than the original threonine residue, interacting with Asn98, Arg164, and Leu165 of GP1, as well as Phe582 of GP2. As predicted based upon previous GP structures, Phe588 rests within a small hydrophobic pocket that is formed by residues in GP1 (Ile33, Leu35, Leu63, and Phe183) and GP2 (Ile584 and Leu585) (Figures 5B and 6). Thus, the crystal structure suggests that Phe588 acts by stabilizing the interface of GP1 and GP2 within one protomer by packing against hydrophobic residues from both subunits.

The N Terminus/Lys588 Interaction Network

To better understand the role of amino acid position 588 on trimer stability, we analyzed the environment of Lys588 in existing crystal and electron microscopy (EM) structures (Figure 6). The Lys588 side chain is located next to a hydrophobic cavity and in direct proximity to the N terminus of GP1 (Figure 6). Understanding of the interaction in this area is obfuscated, because most solved EM and X-ray structures contain a non-native N terminus because of fusion with purification tags, and some proteins were crystallized at a pH at which the N terminus may be deprotonated (see Table S3). Of 25 structures, only four contain the native N terminus and do not contain a heterologous trimerization domain. Two of these structures, 5KEL and 5KEN, do not have the flexible β2-β3 loop directly constrained by an antibody and thus are most representative of the native state of the GP. In both structures, Lys588 is close to the N terminus. Because this arrangement seems to be destabilizing, we tested the trimer stability of GP variants with and without an N-terminal extension. The GP variant with a native GP1 N terminus has a lower trimer yield compared with a variant in which the N terminus was elongated by addition of five amino acids ETGRS, used in most crystallized GP proteins (Figure 7).

We analyzed the interactions around amino acid 588 in the previously determined cryo-EM structure (PDB: 5KEL). In the cryo-EM structure, the wild-type lysine side chain was built in an orientation that suggests interaction between the lysine's amino group and the N terminus. However, the density in this region is weak, and an alternative conformation with the lysine packed into the neighboring hydrophobic pocket could be possible (Figure 6C). Interestingly, both arrangements are energetically unfavorable, involving positive charge repulsion or desolvation of the lysine's amino group, suggesting Lys588 and the N terminus are trapped in a metastable conformation. We believe the N-terminal extension, which does not alter the position of Ile33 in the structure (Figure 7C), effectively decreases the instability arising because of the repulsive interaction of the native N terminus with Lys588 and as a result improves the stability of GP trimers. Mutation of Lys588, as in the K588F variant described here, achieves the same task, but simultaneously fills the neighboring hydrophobic cavity. This seems to result in larger improvement of the protein's stability and expression than removal of the electrostatic repulsion only (Figure 7) and even stabilizes GP with an extended N terminus (see the last panel of Figure 4A showing GP with an N-terminal HA tag), although to a lesser extent than GP without an extended N terminus. The improvement in both cases stems from eliminating the

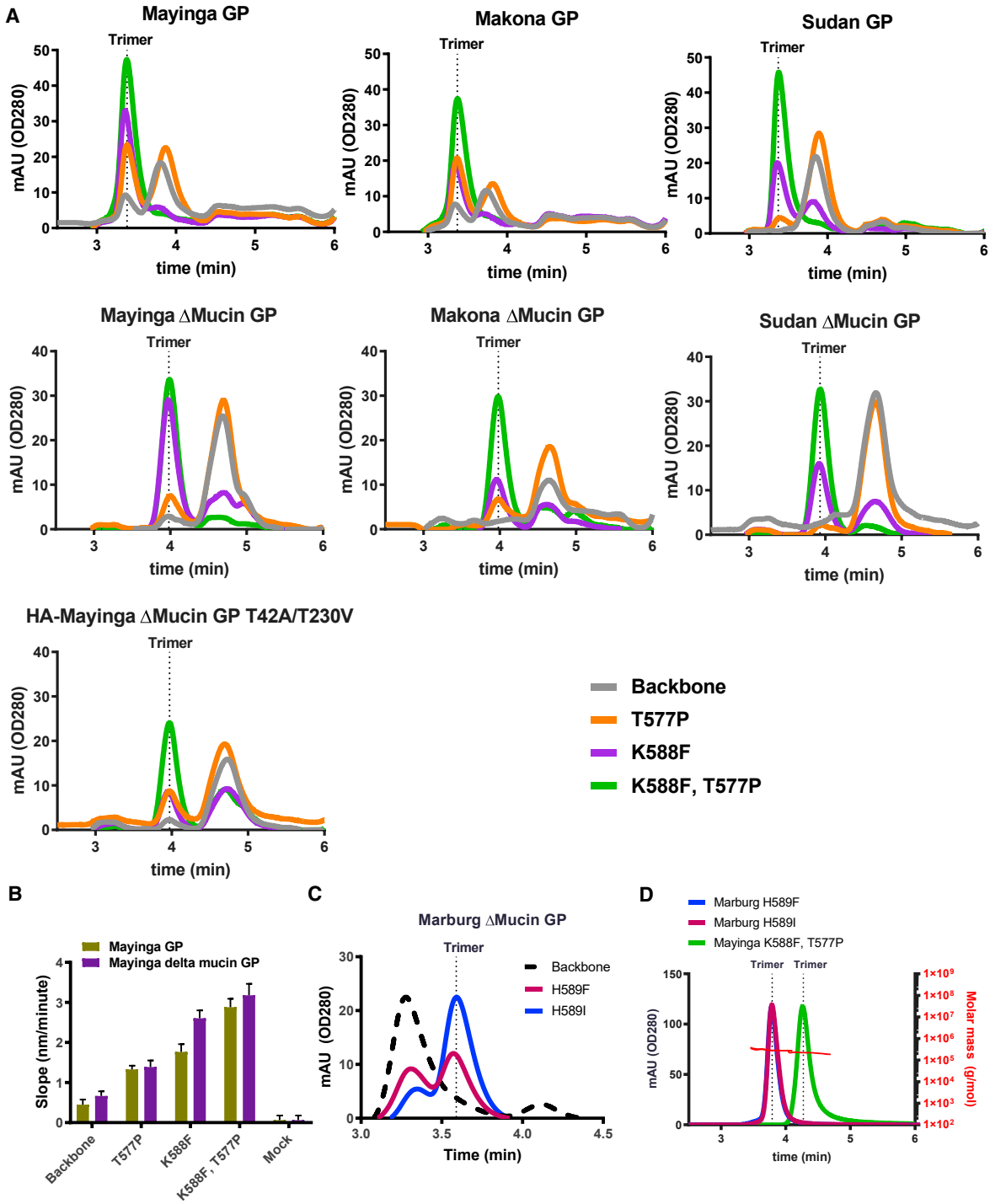

Figure 4. Increase in Trimer Formation after Combination of K588F and T577P in Mayinga, Makona, and SUDV GPs and Trimer Increase in Marburg GP after H589I/F Substitution

(A) Analytical SEC profiles of Ebola GP, Ebola Δmucin GP, and HA-Mayinga Δmucin GP with T577P and/or K588F substitutions. Analysis was performed on crude cell culture supernatant 3 days after transient transfection. The trimer peak is indicated with a dashed line labeled Trimer.

(B) BLI binding rates at 10 s of binding of monoclonal mAb100. Data are represented as mean ± SEM.

(C) Analytical SEC signals of crude cell culture supernatants of the Marburg Δmucin GPs.

(D) SEC-MALS with purified Marburg Δmucin and Mayinga Δmucin GP trimers. The red lines show the molar mass traces (right y axis). The dn/dc values used are 0.185 for all three trimers.

See also Figures S1 and S5.

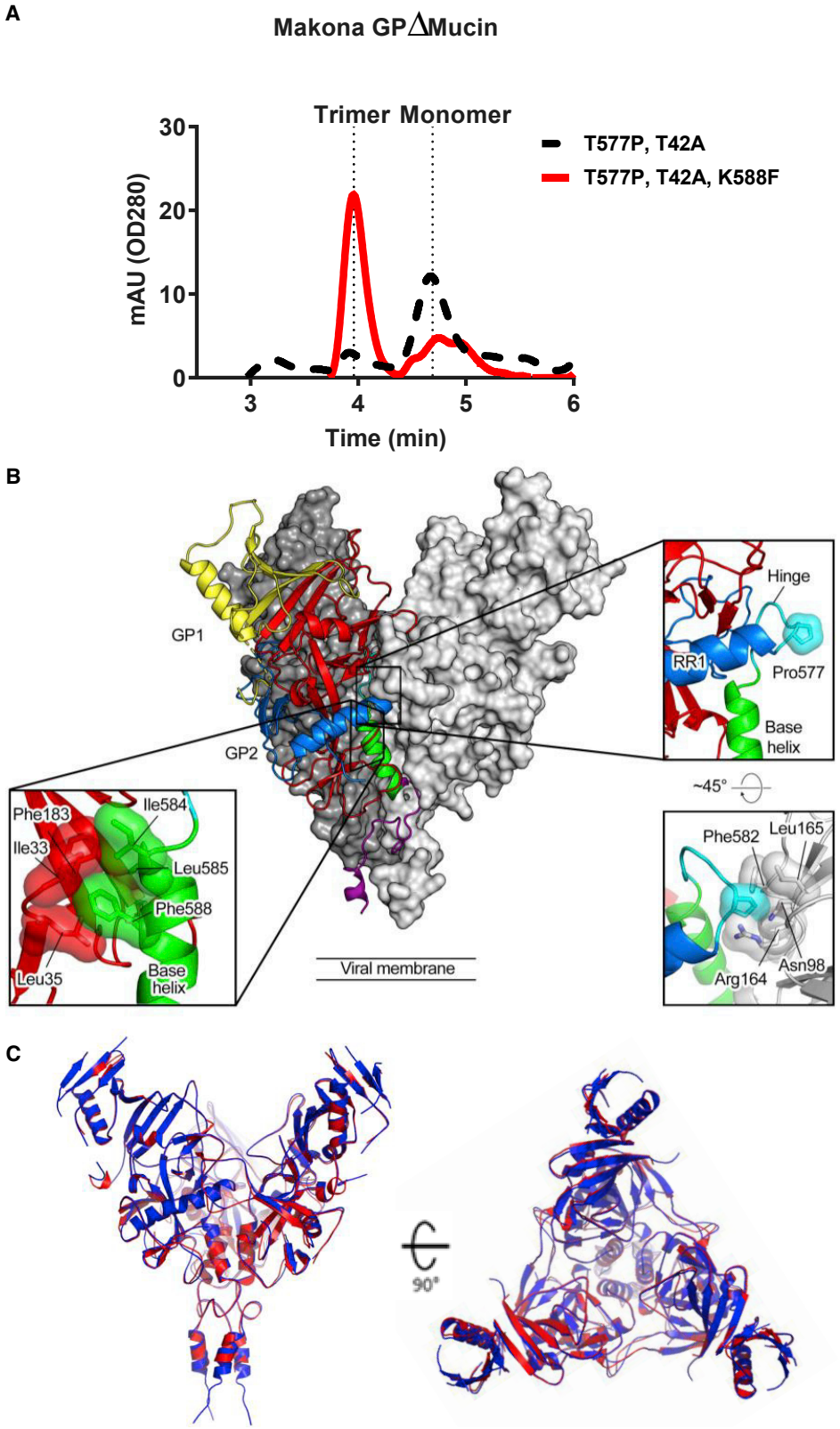

(legend on next page)

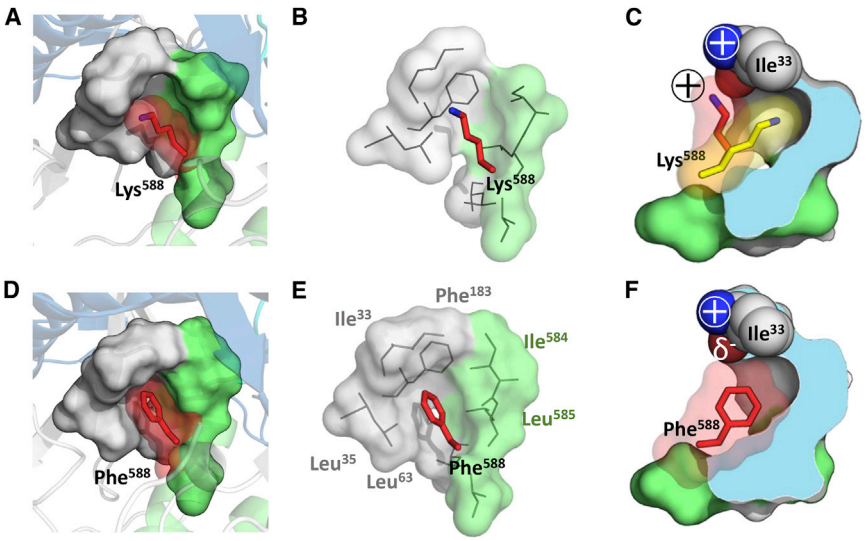

Figure 6. Interactions of Lys or Phe at Position 588 with the Ebola GP

(A–C) Wild-type structures determined by cryo-EM (PDB: 5KEL).

(A) Packing of the Lys588 side chain (red) against the hydrophobic pocket composed of the base helix (green) and GP1 (gray).

(B) Residues forming the pocket, including the N terminus of GP1.

(C) Side view of the pocket. Lys588 can either fill the space in the hydrophobic pocket (yellow rotamer) or form a polar interaction with the backbone of the N-terminal Ile33 (red rotamer). Neither solution is energetically favorable (proximity of positive charges versus desolvation of the positive charge).

(D–F) K588F pocket based on the crystal structure.

(D) Phe588 (red) tightly packed in the hydrophobic pocket.

(E) All residues forming the pocket and hydrophobic interactions with Phe588.

(F) Side view on the K588F pocket. Positive charge proximity is removed, and the sidechain of Phe588 is buried in the pocket.

high energy conformation, which may be involved in the prefusion to postfusion refolding process.

DISCUSSION

Like other class I fusion proteins, Ebola GP refolds from the prefusion to the postfusion state. However, for Ebola GP, the requirements for entry are unusually complex, and most details of the refolding process are unknown. Strategies to stabilize GP in the native soluble prefusion trimeric state have not been described. Production of native trimeric Ebola GP ectodomain is challenging, because most of the protein is monomeric. In recent years, structural knowledge of class I fusion proteins has greatly informed the design of mutations to stabilize these metastable proteins. Introduction of cavity-filling residues and disulfide bridges has been successful in a range of fusion proteins (Hastie et al., 2017; McLellan et al., 2013; Stewart-Jones et al., 2018). Introduction of glycine residues (Guenaga et al., 2017) or a single proline that restricts the movement of the hinge loop in RR1 and prevents the central helix extension and consequential release of the fusion peptide has also been successful, as was shown for RSV F, HIV Env, human metapneumo virus F, Lassa GP, and Middle Eastern respiratory syndrome coronavirus S (Battles et al., 2017; Hastie et al., 2017; Krarup et al., 2015; Pallesen et al., 2017). The substitution of buried or partially buried charged residues with hydrophobic residues resulted in the stabilization of HIV Env (Rutten et al., 2018). Here, the T577P substitution in the hinge loop of RR1 and substitution of the partially buried charged residue Lys588 with a hydrophobic residue in the base helix at the GP1-GP2 interface stabilized the soluble GP trimer and led to a ~20-fold increase in trimer production. The proline substitution increased stability and expression of several Ebola GPs, and the substitution of the buried charged residue increased stability and expression of Ebola GP and Marburg GP and thus may be universally applied to filoviruses.

Our results point toward Lys588 as an important contributor to the instability of Ebola GP trimers. Not only is Lys588 partially buried, but it is also restrained to interact with a positively charged N terminus (Figures 6A–6C). Such an unstable, high-energy configuration implies the region could act as a structural switch for undergoing conformational change. In the unstable region around Lys588, the N terminus of GP1 can move, as opposed to the lysine, which is fixed on the base helix. Exit of the N terminus may compromise its interaction with the intraprotomeric α3 helix (HR1) of RR1 that contains the internal fusion loop. This HR1 helix is stabilized by Pro34 and by several of the residues that form the hydrophobic pocket (Ile584, Phe183 and the N-terminal GP1 Ile33 residue). Loss of the Ile33-Lys588 interaction would release the N-terminal Ile33, break up the hydrophobic pocket, and thereby disrupt contacts with HR1 in the refolding region. Removal of the instability by mutating the N terminus results in improved expression and trimer stability. An alternative way to remove the instability is by mutating the lysine to a hydrophobic residue, as described

Figure 5. Crystal Structure of Stabilized Makona ΔMucin GP

(A) Analytical SEC profile of the crude cell culture supernatant of the T577P/T42A/K588F Makona Δmucin GP that was used for crystallization and a variant lacking K588F.

(B) GP is viewed along the viral membrane, with two protomers shown as gray molecular surfaces and the other protomer shown as ribbons colored according to the schematic in Figure 1A. Insets show the regions surrounding Phe588 (left) and Pro577 (right), with side chains shown as sticks with transparent molecular surfaces. Nitrogen and oxygen atoms are colored blue and red, respectively.

(C) Superposed GP structures of Mayinga Δmucin GP (5JQ3) in blue and stabilized Makona Δmucin GP in red: side view (left) and top view (right).

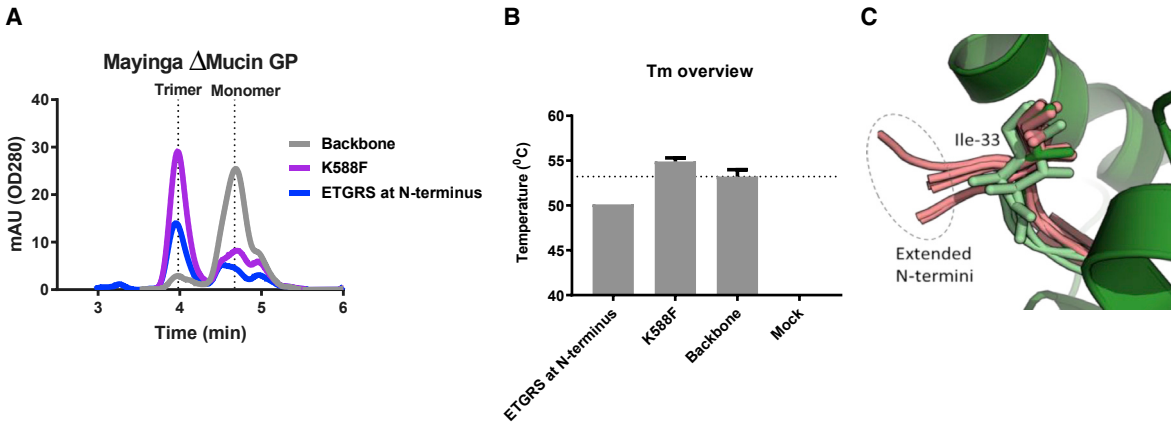

Figure 7. Stability and Trimer Content of Mayinga ΔMucin GP Variants

(A) Analytical SEC profile of variants with K588F mutation and N-terminal ETGRS extension. Analysis was performed on crude cell culture supernatant.

(B) Analysis of T_m using differential scanning fluorometry (DSF) on variants with N-terminal extension and the K588F variant. Data are represented as mean ± SEM.

(C) Superposed structures with the native N terminus (stabilized Makona Δmucin GP structure in dark green; 5KEL, 5KEN, and 6DZM in green) and structures with extended N termini (6F5U, 6G9I, 5F1B, 5HJ3, 3S88, 3VE0, 3CSY, and 6EAY in pink).

in this study. The K588F mutation not only removes the excess positive charge in the region but also adds favorable interactions with a neighboring hydrophobic pocket composed of residues from both GP1 and GP2 subunits (Figures 6D–6F and 7), which also seems to contribute to the stability substantially, given that K588A does not result in substantially increased trimer yields (Figures 3B and 3D).

Interestingly, the K588F mutation described here for Ebola GP has some resemblance to the D589V mutation used to stabilize HIV Env (Rutten et al., 2018). Both substitutions increase trimer yield and are located in the base helix of the fusion domain (GP2 in filovirus GP and gp41 in HIV Env). Both also make an intraprotomeric interaction with the head domain (GP1 and gp120), which forms a hydrophobic pocket. These similarities reported here suggest commonalities in the triggering mechanisms of Ebola GP and HIV Env and indicate that the strategy used here to stabilize GP may be broadly applicable to other class I viral fusion proteins.

In conclusion, stabilization of the hinge loop in RR1 by T577P and stabilization and neutralization of a region of instability in the GP1-GP2 interface by K588F dramatically increases the yield of filovirus prefusion GP trimers. The increasing knowledge of the refolding mechanism of class I fusion proteins is critical for the design of stable proteins that can be used for vaccines, diagnostics, or isolation of antibodies.

STAR★METHODS

Detailed methods are provided in the online version of this paper and include the following:

- KEY RESOURCES TABLE
- LEAD CONTACT AND MATERIALS AVAILABILITY
- EXPERIMENTAL MODEL AND SUBJECT DETAILS
  - Cell Lines
- METHOD DETAILS
  - Expression Plasmids and Transient Transfections
  - Purification of Ebola or Marburg GP Protein
  - Antibody production and purification
  - NativePAGE Analysis
  - Analytical SEC and SEC-MALS
  - BioLayer Interferometry (BLI)
  - Differential scanning fluorometry (DSF)
  - Differential scanning calorimetry (DSC)
  - Crystal structure determination
- QUANTIFICATION AND STATISTICAL ANALYSIS
- DATA AND CODE AVAILABILITY

SUPPLEMENTAL INFORMATION

Supplemental Information can be found online at https://doi.org/10.1016/j.celrep.2020.03.025.

ACKNOWLEDGMENTS

We thank Mark Bakkers for suggestions and critically reading the manuscript and Ava Sadi and Mark Luinenburg for technical support. These studies were funded by Janssen Vaccines & Prevention.

AUTHOR CONTRIBUTIONS

Conceptualization, L.R. and J.P.M.L.; Methodology, L.R. and S.B.; Investigation, S.B., J.J., and M.S.A.G.; Writing – Original Draft, L.R., S.B., M.S.A.G., J.J., J.S.M., and J.P.M.L.; Writing – Review & Editing, L.R., S.B., M.S.A.G., J.S.M., and J.P.M.L.; Supervision, L.R., J.S.M., and J.P.M.L.

DECLARATION OF INTERESTS

L.R., S.B., J.J., and J.P.M.L. are employees at Janssen Vaccines & Prevention. L.R., S.B., and J.P.M.L. are inventors on an international patent application describing trimer stabilizing Ebola GP mutations. J.P.M.L. holds stock in Johnson & Johnson. The remaining authors declare no competing financial interests.

Received: August 21, 2019
Revised: January 27, 2020
Accepted: March 10, 2020
Published: March 31, 2020

REFERENCES

Adams, P.D., Grosse-Kunstleve, R.W., Hung, L.W., Ioerger, T.R., McCoy, A.J., Moriarty, N.W., Read, R.J., Sacchettini, J.C., Sauter, N.K., and Terwilliger, T.C. (2002). PHENIX: building new software for automated crystallographic structure determination. Acta Crystallogr. D Biol. Crystallogr. *58*, 1948–1954.

Alvarez, C.P., Lasala, F., Carrillo, J., Muñiz, O., Corbí, A.L., and Delgado, R. (2002). C-type lectins DC-SIGN and L-SIGN mediate cellular entry by Ebola virus in *cis* and in *trans*. J. Virol. *76*, 6841–6844.

Bale, S., Dias, J.M., Fusco, M.L., Hashiguchi, T., Wong, A.C., Liu, T., Keuhne, A.I., Li, S., Woods, V.L., Jr., Chandran, K., et al. (2012). Structural basis for differential neutralization of ebolaviruses. Viruses *4*, 447–470.

Battles, M.B., Más, V., Olmedillas, E., Cano, O., Vázquez, M., Rodríguez, L., Melero, J.A., and McLellan, J.S. (2017). Structure and immunogenicity of pre-fusion-stabilized human metapneumovirus F glycoprotein. Nat. Commun. *8*, 1528.

Binley, J.M., Sanders, R.W., Clas, B., Schuelke, N., Master, A., Guo, Y., Kajumo, F., Anselma, D.J., Maddon, P.J., Olson, W.C., and Moore, J.P. (2000). A recombinant human immunodeficiency virus type 1 envelope glycoprotein complex stabilized by an intermolecular disulfide bond between the gp120 and gp41 subunits is an antigenic mimic of the trimeric virion-associated structure. J. Virol. *74*, 627–643.

Bornholdt, Z.A., Ndungo, E., Fusco, M.L., Bale, S., Flyak, A.I., Crowe, J.E., Jr., Chandran, K., and Saphire, E.O. (2016). Host-Primed Ebola Virus GP Exposes a Hydrophobic NPC1 Receptor-Binding Pocket, Revealing a Target for Broadly Neutralizing Antibodies. MBio *7*, e02154–15.

Brindley, M.A., Hunt, C.L., Kondratowicz, A.S., Bowman, J., Sinn, P.L., McCray, P.B., Jr., Quinn, K., Weller, M.L., Chiorini, J.A., and Maury, W. (2011). Tyrosine kinase receptor Axl enhances entry of *Zaire ebolavirus* without direct interactions with the viral glycoprotein. Virology *415*, 83–94.

Carette, J.E., Raaben, M., Wong, A.C., Herbert, A.S., Obernosterer, G., Mulherkar, N., Kuehne, A.I., Kranzusch, P.J., Griffin, A.M., Ruthel, G., et al. (2011). Ebola virus entry requires the cholesterol transporter Niemann-Pick C1. Nature *477*, 340–343.

Chandran, K., Sullivan, N.J., Felbor, U., Whelan, S.P., and Cunningham, J.M. (2005). Endosomal proteolysis of the Ebola virus glycoprotein is necessary for infection. Science *308*, 1643–1645.

Collaborative Computational Project, Number 4 (1994). The CCP4 suite: programs for protein crystallography. Acta Crystallogr. D Biol. Crystallogr. *50*, 760–763.

Corti, D., Misasi, J., Mulangu, S., Stanley, D.A., Kanekiyo, M., Wollen, S., Ploquin, A., Doria-Rose, N.A., Staupe, R.P., Bailey, M., et al. (2016). Protective monotherapy against lethal Ebola virus infection by a potently neutralizing antibody. Science *351*, 1126.

Côté, M., Misasi, J., Ren, T., Bruchez, A., Lee, K., Filone, C.M., Hensley, L., Li, Q., Ory, D., Chandran, K., and Cunningham, J. (2011). Small molecule inhibitors reveal Niemann-Pick C1 is essential for Ebola virus infection. Nature *477*, 344–348.

Dias, J.M., Kuehne, A.I., Abelson, D.M., Bale, S., Wong, A.C., Halfmann, P., Muhammad, M.A., Fusco, M.L., Zak, S.E., Kang, E., et al. (2011). A shared structural solution for neutralizing ebolaviruses. Nat. Struct. Mol. Biol. *18*, 1424–1427.

Emsley, P., and Cowtan, K. (2004). Coot: model-building tools for molecular graphics. Acta Crystallogr. D Biol. Crystallogr. *60*, 2126–2132.

Evans, P.R., and Murshudov, G.N. (2013). How good are my data and what is the resolution? Acta Crystallogr. D Biol. Crystallogr. *69*, 1204–1214.

Fels, J.M., Spence, J.S., Bortz, R.H., 3rd, Bornholdt, Z.A., and Chandran, K. (2019). A Hyperstabilizing Mutation in the Base of the Ebola Virus Glycoprotein Acts at Multiple Steps To Abrogate Viral Entry. MBio *10*, e01408–e01419.

Fénéant, L., Szymańska-de Wijs, K.M., Nelson, E.A., and White, J.M. (2019). An exploration of conditions proposed to trigger the Ebola virus glycoprotein for fusion. PLoS ONE *14*, e0219312.

Guenaga, J., Garces, F., de Val, N., Stanfield, R.L., Dubrovskaya, V., Higgins, B., Carrette, B., Ward, A.B., Wilson, I.A., and Wyatt, R.T. (2017). Glycine Substitution at Helix-to-Coil Transitions Facilitates the Structural Determination of a Stabilized Subtype C HIV Envelope Glycoprotein. Immunity *46*, 792–803.

Hastie, K.M., Zandonatti, M.A., Kleinfelter, L.M., Heinrich, M.L., Rowland, M.M., Chandran, K., Branco, L.M., Robinson, J.E., Garry, R.F., and Saphire, E.O. (2017). Structural basis for antibody-mediated neutralization of Lassa virus. Science *356*, 923–928.

International Committee on Taxonomy of Viruses (2019). Genus: Ebolavirus. talk.ictvonline.org/ictv-reports/ictv_online_report/negative-sense-rna-viruses/mononegavirales/w/filoviridae/1086/genus-ebolavirus.

Janus, B.M., van Dyk, N., Zhao, X., Howell, K.A., Soto, C., Aman, M.J., Li, Y., Fuerst, T.R., and Ofek, G. (2018). Structural basis for broad neutralization of ebolaviruses by an antibody targeting the glycoprotein fusion loop. Nat. Commun. *9*, 3934.

Jemielity, S., Wang, J.J., Chan, Y.K., Ahmed, A.A., Li, W., Monahan, S., Bu, X., Farzan, M., Freeman, G.J., Umetsu, D.T., et al. (2013). TIM-family proteins promote infection of multiple enveloped viruses through virion-associated phosphatidylserine. PLoS Pathog. *9*, e1003232.

Kondratowicz, A.S., Lennemann, N.J., Sinn, P.L., Davey, R.A., Hunt, C.L., Moller-Tank, S., Meyerholz, D.K., Rennert, P., Mullins, R.F., Brindley, M., et al. (2011). T-cell immunoglobulin and mucin domain 1 (TIM-1) is a receptor for *Zaire Ebolavirus* and Lake Victoria *Marburgvirus*. Proc. Natl. Acad. Sci. USA *108*, 8426–8431.

Krarup, A., Truan, D., Furmanova-Hollenstein, P., Bogaert, L., Bouchier, P., Bisschop, I.J.M., Widjojoatmodjo, M.N., Zahn, R., Schuitemaker, H., McLellan, J.S., and Langedijk, J.P.M. (2015). A highly stable prefusion RSV F vaccine derived from structural analysis of the fusion mechanism. Nat. Commun. *6*, 8143.

Kuhn, J.H., Adachi, T., Adhikari, N.K.J., Arribas, J.R., Bah, I.E., Bausch, D.G., Bhadelia, N., Borchert, M., Brantsæter, A.B., Brett-Major, D.M., et al. (2019). New filovirus disease classification and nomenclature. Nat. Rev. Microbiol. *17*, 261–263.

Lee, J.E., Fusco, M.L., Hessell, A.J., Oswald, W.B., Burton, D.R., and Saphire, E.O. (2008). Structure of the Ebola virus glycoprotein bound to an antibody from a human survivor. Nature *454*, 177–182.

McCoy, A.J., Grosse-Kunstleve, R.W., Adams, P.D., Winn, M.D., Storoni, L.C., and Read, R.J. (2007). Phaser crystallographic software. J. Appl. Cryst. *40*, 658–674.

McLellan, J.S., Chen, M., Joyce, M.G., Sastry, M., Stewart-Jones, G.B., Yang, Y., Zhang, B., Chen, L., Srivatsan, S., Zheng, A., et al. (2013). Structure-based design of a fusion glycoprotein vaccine for respiratory syncytial virus. Science *342*, 592–598.

Miller, E.H., Obernosterer, G., Raaben, M., Herbert, A.S., Deffieu, M.S., Krishnan, A., Ndungo, E., Sandesara, R.G., Carette, J.E., Kuehne, A.I., et al. (2012). Ebola virus entry requires the host-programmed recognition of an intracellular receptor. EMBO J. *31*, 1947–1960.

Morin, A., Eisenbraun, B., Key, J., Sanschagrin, P.C., Timony, M.A., Ottaviano, M., and Sliz, P. (2013). Collaboration gets the most out of software. eLife *2*, e01456.

Mulherkar, N., Raaben, M., de la Torre, J.C., Whelan, S.P., and Chandran, K. (2011). The Ebola virus glycoprotein mediates entry via a non-classical dynamin-dependent macropinocytic pathway. Virology *419*, 72–83.

Murin, C.D., Bruhn, J.F., Bornholdt, Z.A., Copps, J., Stanfield, R., and Ward, A.B. (2018). Structural Basis of Pan-Ebolavirus Neutralization by an Antibody Targeting the Glycoprotein Fusion Loop. Cell Rep. *24*, 2723–2732.

Nanbo, A., Imai, M., Watanabe, S., Noda, T., Takahashi, K., Neumann, G., Halfmann, P., and Kawaoka, Y. (2010). Ebolavirus is internalized into host cells via macropinocytosis in a viral glycoprotein-dependent manner. PLoS Pathog. *6*, e1001121.

Pallesen, J., Murin, C.D., de Val, N., Cottrell, C.A., Hastie, K.M., Turner, H.L., Fusco, M.L., Flyak, A.I., Zeitlin, L., Crowe, J.E., Jr., et al. (2016). Structures of Ebola virus GP and sGP in complex with therapeutic antibodies. Nat. Microbiol. *1*, 16128.

Pallesen, J., Wang, N., Corbett, K.S., Wrapp, D., Kirchdoerfer, R.N., Turner, H.L., Cottrell, C.A., Becker, M.M., Wang, L., Shi, W., et al. (2017). Immunogenicity and structures of a rationally designed prefusion MERS-CoV spike antigen. Proc. Natl. Acad. Sci. USA *114*, E7348–E7357.

Potterton, E., Briggs, P., Turkenburg, M., and Dodson, E. (2003). A graphical user interface to the CCP4 program suite. Acta Crystallogr. D Biol. Crystallogr. *59*, 1131–1137.

Powell, H.R., Battye, T.G.G., Kontogiannis, L., Johnson, O., and Leslie, A.G.W. (2017). Integrating macromolecular X-ray diffraction data with the graphical user interface iMosflm. Nat. Protoc. *12*, 1310–1325.

Rutten, L., Lai, Y.T., Blokland, S., Truan, D., Bisschop, I.J.M., Strokappe, N.M., Koornneef, A., van Manen, D., Chuang, G.Y., Farney, S.K., et al. (2018). A Universal Approach to Optimize the Folding and Stability of Prefusion-Closed HIV-1 Envelope Trimers. Cell Rep. *23*, 584–595.

Saeed, M.F., Kolokoltsov, A.A., Albrecht, T., and Davey, R.A. (2010). Cellular entry of Ebola virus involves uptake by a macropinocytosis-like mechanism and subsequent trafficking through early and late endosomes. PLoS Pathog. *6*, e1001110.

Sanders, R.W., Vesanen, M., Schuelke, N., Master, A., Schiffner, L., Kalyanaraman, R., Paluch, M., Berkhout, B., Maddon, P.J., Olson, W.C., et al. (2002). Stabilization of the soluble, cleaved, trimeric form of the envelope glycoprotein complex of human immunodeficiency virus type 1. J. Virol. *76*, 8875–8889.

Schornberg, K., Matsuyama, S., Kabsch, K., Delos, S., Bouton, A., and White, J. (2006). Role of endosomal cathepsins in entry mediated by the Ebola virus glycoprotein. J. Virol. *80*, 4174–4178.

Shimojima, M., Ikeda, Y., and Kawaoka, Y. (2007). The mechanism of Axl-mediated Ebola virus infection. J. Infect. Dis. *196* (*Suppl 2*), S259–S263.

Simmons, G., Reeves, J.D., Grogan, C.C., Vandenberghe, L.H., Baribaud, F., Whitbeck, J.C., Burke, E., Buchmeier, M.J., Soilleux, E.J., Riley, J.L., et al. (2003). DC-SIGN and DC-SIGNR bind Ebola glycoproteins and enhance infection of macrophages and endothelial cells. Virology *305*, 115–123.

Stewart-Jones, G.B.E., Chuang, G.Y., Xu, K., Zhou, T., Acharya, P., Tsybovsky, Y., Ou, L., Zhang, B., Fernandez-Rodriguez, B., Gilardi, V., et al. (2018). Structure-based design of a quadrivalent fusion glycoprotein vaccine for human parainfluenza virus types 1–4. Proc. Natl. Acad. Sci. USA *115*, 12265–12270.

Takada, A., Watanabe, S., Ito, H., Okazaki, K., Kida, H., and Kawaoka, Y. (2000). Downregulation of beta1 integrins by Ebola virus glycoprotein: implication for virus entry. Virology *278*, 20–26.

Wang, J., Rho, S.H., Park, H.H., and Eom, S.H. (2005). Correction of X-ray intensities from an HslV-HslU co-crystal containing lattice-translocation defects. Acta Crystallogr. D Biol. Crystallogr. *61*, 932–941.

Wang, H., Shi, Y., Song, J., Qi, J., Lu, G., Yan, J., and Gao, G.F. (2016). Ebola Viral Glycoprotein Bound to Its Endosomal Receptor Niemann-Pick C1. Cell *164*, 258–268.

West, B.R., Moyer, C.L., King, L.B., Fusco, M.L., Milligan, J.C., Hui, S., and Saphire, E.O. (2018). Structural Basis of Pan-Ebolavirus Neutralization by a Human Antibody against a Conserved, yet Cryptic Epitope. MBio *9*, e01674-18.

World Health Organization (2020a). Ebola outbreak 2014–2016. www.who.int/csr/disease/ebola/en/.

World Health Organization (2020b). Ebola in the Democratic Republic of the Congo Health Emergency Update. www.who.int/emergencies/diseases/ebola/drc-2019.

Zhao, Y., Ren, J., Harlos, K., Jones, D.M., Zeltina, A., Bowden, T.A., Padilla-Parra, S., Fry, E.E., and Stuart, D.I. (2016). Toremifene interacts with and destabilizes the Ebola virus glycoprotein. Nature *535*, 169–172.

STAR★METHODS

KEY RESOURCES TABLE

REAGENT or RESOURCE	SOURCE	IDENTIFIER
Antibodies		
mAb100	Corti et al., 2016	N/A
Chemicals, Peptides, and Recombinant Proteins		
CHT type 1 resin	Bio-Rad	Cat# 158-4000
HisTrap HP 5 mL	GEHC	Cat#17524802
HiLoad Superdex 200 16/600 size-exclusion column	GEHC	Cat# 28989335
mAb Select SuRe 5 mL HiTrap	GEHC	Cat# 11003495
HiPrep 26/10 Desalting column	GEHC	Cat# 17508701
anti-hIgG (AHC) sensors	FortéBio	cat#18-1092
Sypro Orange dye	Thermo Fisher Scientific	Cat# S6650
Critical Commercial Assays		
50K Amicon Ultra concentrators	Millipore	Cat# UFC905024
NativePage Bis-Tris gradient gels 4-16%	LifeTechnologies	Cat# BN1002BOX
Deposited Data		
Stabilized Makona Δ-mucin GP X-ray structure	This paper	PDB: 6VKM
Experimental Models: Cell Lines		
Human: Expi293F	Thermo Fischer Scientific	Cat#A14527
Software and Algorithms		
FortéBio Data Analysis 8.1 software	FortéBio	
CCP4i interface	Morin et al., 2013; Potterton et al., 2003	https://www.ccp4.ac.uk/ccp4i_main.php
iMOSFLM	Powell et al., 2017	https://www.mrc-lmb.cam.ac.uk/mosflm/imosflm/ver730/installation.html
AIMLESS	Evans and Murshudov, 2013	http://www.ccp4.ac.uk/dist/html/aimless.html
PHASER	McCoy et al., 2007	https://www.phenix-online.org/documentation/reference/phaser_mr.html
Coot	Emsley and Cowtan, 2004	https://www2.mrc-lmb.cam.ac.uk/personal/pemsley/coot/
PHENIX	Adams et al., 2002	
Astra 7.3 software package		https://www.wyatt.com/products/software/astra.html
Chromeleon 7.2.8.0 software package		https://www.thermofisher.com/order/catalog/product/CHROMELEON7

LEAD CONTACT AND MATERIALS AVAILABILITY

This study did not generate new unique reagents. All requests for reagents and resources should be directed to the lead contact, Johannes P.M. Langedijk (hlangedi@its.jnj.com).

EXPERIMENTAL MODEL AND SUBJECT DETAILS

Cell Lines

Human Expi293F cells (Thermo Fischer Scientific) were maintained in Expi293 Expression medium (Thermo Fisher Scientific).

METHOD DETAILS

Expression Plasmids and Transient Transfections

The Mayinga and Makona GP proteins contain amino acids 1-647 followed by a His6-tag. For the Mayinga and Sudan (Gulu) GP protein without the mucin-like domain, amino acids 320 until 476 were deleted and for the Makona protein without the mucin-like domain, amino acids 314 until 472 were deleted. DNA encoding the glycoproteins (GPs) were synthesized and codon-optimized for expression in human cells at GenScript (Piscataway, NJ 08854). The codon-optimized sequences were then cloned into the vector pcDNA2004 to generate the GP constructs, which were used as the backbone sequences for introducing further mutations. The genes were expressed in Expi293F cells (Thermo Fischer) according to the manufacturer's specification. Glucose levels were monitored using the ViCell MetaFlex (Beckmann). Glucose was depleted at day 4 post-transfection and therefore glucose was added at a 15 mM concentration. Supernatants were harvested at day 6 post-transfection by centrifugation and sterile filtration. For small scale 96-well format for analytical SEC experiment, the supernatants were harvested 3 days post-transfection.

Purification of Ebola or Marburg GP Protein

Interfering host-cell proteins (HCPs) were scavenged by applying the supernatant to 13 mL CHT type 1 resin (Biorad) in an XK16/20 column (GEHC) using a flow rate of 300 cm/hr and a running buffer of 5 mM NaPO4, pH 6.8. Bound proteins were eluted by a step elution using 500 mM NaPO4, pH 7.4. The HCP depleted flow through was subsequently applied to a HisTrap HP 5 mL (GEHC) using a flow rate of 300 cm/hr and a running buffer of 20 mM Tris, 500 mM NaCl pH 7.4. Bound proteins were eluted using a step gradient of 15, 30 and 100% elution buffer (20 mM Tris, 500 mM NaCl, 300 mM imidazole pH 7.4) while running the column in upflow with a flow rate of 600 cm/hr. The trimer fractions eluted along with aggregates when 100 mM imidazole was applied. This fraction was concentrated, using 50K Amicon Ultra concentrators (Millipore), and applied to a Superdex 16/600 size-exclusion column (GEHC) using a flow rate of 60 cm/hr to separate the trimer fraction from aggregates and monomers. The fractions containing the trimer peak were pooled, and the identity of the peak confirmed as GP protein using SDS-PAGE, and/or SEC-MALS analysis. The concentration of the purified Ebola or Marburg GP was determined by measuring the optical density at 280 nm, and the purified protein was stored at 4°C until further use.

Antibody production and purification

The heavy and light chain of mAb100 were cloned into a single IgG1 expression vector to express a fully human IgG1 antibody. mAb100 was made by transfecting the IgG1 expression construct using the ExpiFectamine 293 Transfection Kit (ThermoFisher) in Expi293F (ThermoFisher) cells according to the manufacturer specifications. mAb100 antibodies were purified from serum-free culture supernatants using mAb Select SuRe resin (GE Healthcare) followed by rapid desalting using a HiPrep 26/10 Desalting column (GE Healthcare). The final formulation buffer was 20 mM NaAc, 75 mM NaCl, 5% Sucrose pH 5.5. IgG quality was confirmed to be > 97% monomeric using SEC-MALS.

NativePAGE Analysis

NativePAGE was performed according to manufacturer's protocol (LifeTechnologies) using 4%–16% NativePage Bis-Tris gradient gels (LifeTechnologies). The GP trimer with mucin-like domain ran at a mass of about 800 kDa, whereas the GP without the mucin-like domain ran at a mass of about 420 kDa.

Analytical SEC and SEC-MALS

The EBOV GP variants were expressed in 96 well format cell cultures. An ultra high-performance liquid chromatography system (Vanquish, Thermo Scientific) and μDAWN TREOS instrument (Wyatt) coupled to an Optilab μT-rEX Refractive Index Detector (Wyatt), in combination with an in-line Nanostar DLS reader (Wyatt), was used for performing the analytical SEC experiment. The cleared crude cell culture supernatants were applied to a TSK-Gel UP-SW3000 4.6x150 mm column with the corresponding guard column (Tosoh Bioscience) equilibrated in running buffer (150 mM sodium phosphate, 50 mM NaCl, pH 7.0) at 0.3 mL/min. When analyzing supernatant samples, μMALS detectors were offline and analytical SEC data was analyzed using Chromeleon 7.2.8.0 software package. The signal of supernatants of non-transfected cells was subtracted from the signal of supernatants of GP transfected cells. When purified proteins were analyzed using SEC-MALS, μMALS detectors were inline and data was analyzed using Astra 7.3 software package. For the protein component, a dn/dc (mL/g) value of 0.1850 was used and for the glycan component a value of 0.1410. Molecular weights were calculated using the RI detector as [C] source and mass recoveries using UV as [C] source.

BioLayer Interferometry (BLI)

A solution of monoclonal antibody mAb100[38] at a concentration of 10 ug/mL was used to immobilize the antibody on anti-hIgG (AHC) sensors (FortéBio cat#18-5060) in 1x kinetics buffer (FortéBio cat#18-1092) in 96-half well black flat bottom polypylene microplates (FortéBio cat#3694). The experiment was performed on an Octet HTX instrument (Pall-FortéBio) at 30 °C with a shaking speed of 1,000 rpm. Activation was 60 s, immobilization of antibodies 600 s, followed by washing for 150 s and then binding the GP proteins for 600 s, and a dissociation of 60 s. The data analysis was performed using the FortéBio Data Analysis 8.1 software (FortéBio). The binding was determined by using association phase analysis. The binding slope was determined at 10 s in nm/minute.

Differential scanning fluorometry (DSF)

The purified protein was mixed with SYPRO orange fluorescent dye (Life Technologies S6650) in a 96-well optical qPCR plate. The optimal dye and protein concentration were determined experimentally. All protein dilutions were performed in PBS, and a negative control sample containing the dye only was used for reference subtraction. The measurement was performed in a qPCR instrument (Applied Biosystems ViiA 7) using a temperature ramp from 25–95°C with a rate of 0.015°C per second. Data were collected continuously. The negative first derivative of the Sypro Orange signal was measured at several intervals during a temperature ramp up to 95°C.

For measurement in supernatants, constructs were expressed in a 96-well format and harvested 3-days post transfection. Samples were diluted with PBS pH 7.4 (GIBCO) containing 8-fold diluted supernatant and 500-fold diluted Sypro Orange dye (5000 x stock, Invitrogen). A mock sample was included as background control. The measurement was performed in a qPCR instrument (Applied Biosystems ViiA 7) using a temperature ramp from 25–95°C with a rate of 0.015°C per second. Data were collected continuously. The negative first derivative was plotted as a function of temperature. The melting temperature corresponds to the lowest point in the curve.

Differential scanning calorimetry (DSC)

Melting temperatures for GPs were determined using MicroCal capillary DSC system. 400 μL of 0.5 mg/mL protein sample was used per measurement. The measurement was performed with a start temperature of 20°C and a final temperature of 110°C. The scan rate 100°C/h and the feedback mode; Low (= signal amplification). The data were analyzed using the Origin J. Software (MicroCal VP-analysis tool).

Crystal structure determination

For crystallization purposes an additional T42A substitution was introduced to remove the glycosylation site at Asn40 (Zhao et al., 2016) and during production a final concentration of 5 μM of kifunensin was used. Although the T577P/T42A variant still has a higher trimer yield than wild-type Makona Δmucin GP, the additional T42A substitution significantly reduced the trimer yield (Figure S3). Deletion of the glycan at position 40 reduced the molecular weight of the monomer as illustrated by the shifted peak in analytical SEC (Figure S3). The trimer retention time, however, was not affected, which may correlate with a relatively compact trimer in the closed prefusion conformation. The stabilized GP T42A/T577P/K588F protein was crystallized by hanging-drop vapor diffusion by mixing 0.5 μL of protein at 8.8 mg/mL with 0.5 μL of water and 1 μL of reservoir solution containing 9.8% polyethylene glycol (PEG) 6000, 0.1 M sodium citrate pH 5.2, and 3% glycerol. Crystals were soaked in reservoir solution supplemented with 25% (v/v) glycerol as a cryoprotectant before being plunge frozen with liquid nitrogen. Data were collected to 3.5 Å resolution at the SBC beamline 19-ID (Advanced Photon Source, Argonne National Laboratory).

X-ray diffraction data were processed using software curated by SBGrid and accessed through the CCP4i interface (Collaborative Computational Project, Number 4, 1994; Morin et al., 2013; Potterton et al., 2003). Data indexing and integration were carried out using iMOSFLM (Powell et al., 2017), and merging and scaling were performed with AIMLESS (Evans and Murshudov, 2013). The results of the L-test identified possible twinning, however, since no merohedral or pseudo-merohedral twin laws are possible for space group *H*32, other possible pathologies were examined. An off-origin peak in the Patterson function with 3.56% the height of the origin peak was identified, suggesting that lattice translocation, which has previously been reported in space group *H*32 (Wang et al., 2005), could be responsible for the deviation from normal data statistics. Uncorrected data were used to determine the molecular replacement solution in PHASER (McCoy et al., 2007) using the previously determined GP structure (PDB ID: 5JQ3) as a search model. One copy of a single GP protomer was present in the asymmetric unit, although weak density for a second overlapping protomer was also visible and is likely the result of the lattice translocation defect. A single copy of the GP protomer was built manually in Coot (Emsley and Cowtan, 2004) and refined in PHENIX (Adams et al., 2002) to an R_{work}/R_{free} of 28.4%/30.3%.

QUANTIFICATION AND STATISTICAL ANALYSIS

Bar graphs of analytical SEC data were presented as mean ± standard error from at least two independent transfections when indicated. Data fitting and statistical analysis was performed using GraphPad Prism software (version 7.00).

DATA AND CODE AVAILABILITY

Atomic coordinates and structure factors for the crystal structure of the stabilized GP trimer have been deposited with the Protein Data Bank with PDB code 6VKM.

Cell Reports, Volume *30*

Supplemental Information

Structure-Based Design of Prefusion-Stabilized Filovirus Glycoprotein Trimers

Lucy Rutten, Morgan S.A. Gilman, Sven Blokland, Jarek Juraszek, Jason S. McLellan, and Johannes P.M. Langedijk

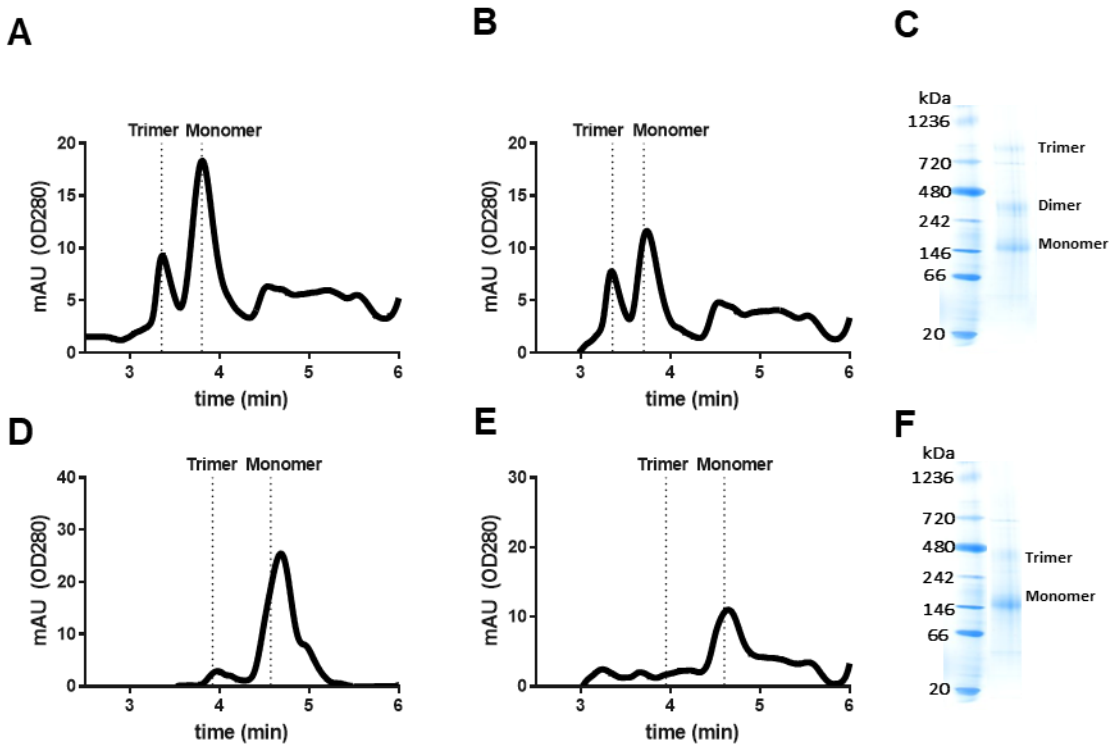

Figure S1. Analysis of soluble wild type Ebola GP proteins performed on crude cell culture supernatant, Related to Figure 4A. Analytical SEC profiles are shown for soluble **A**) Mayinga GP, **B**) Makona GP, **D**) Mayinga ∆mucin GP, **E**) Makona ∆mucin GP. Blue native PAGE for Makona GP **C**) and Makona ∆mucin GP **F**)

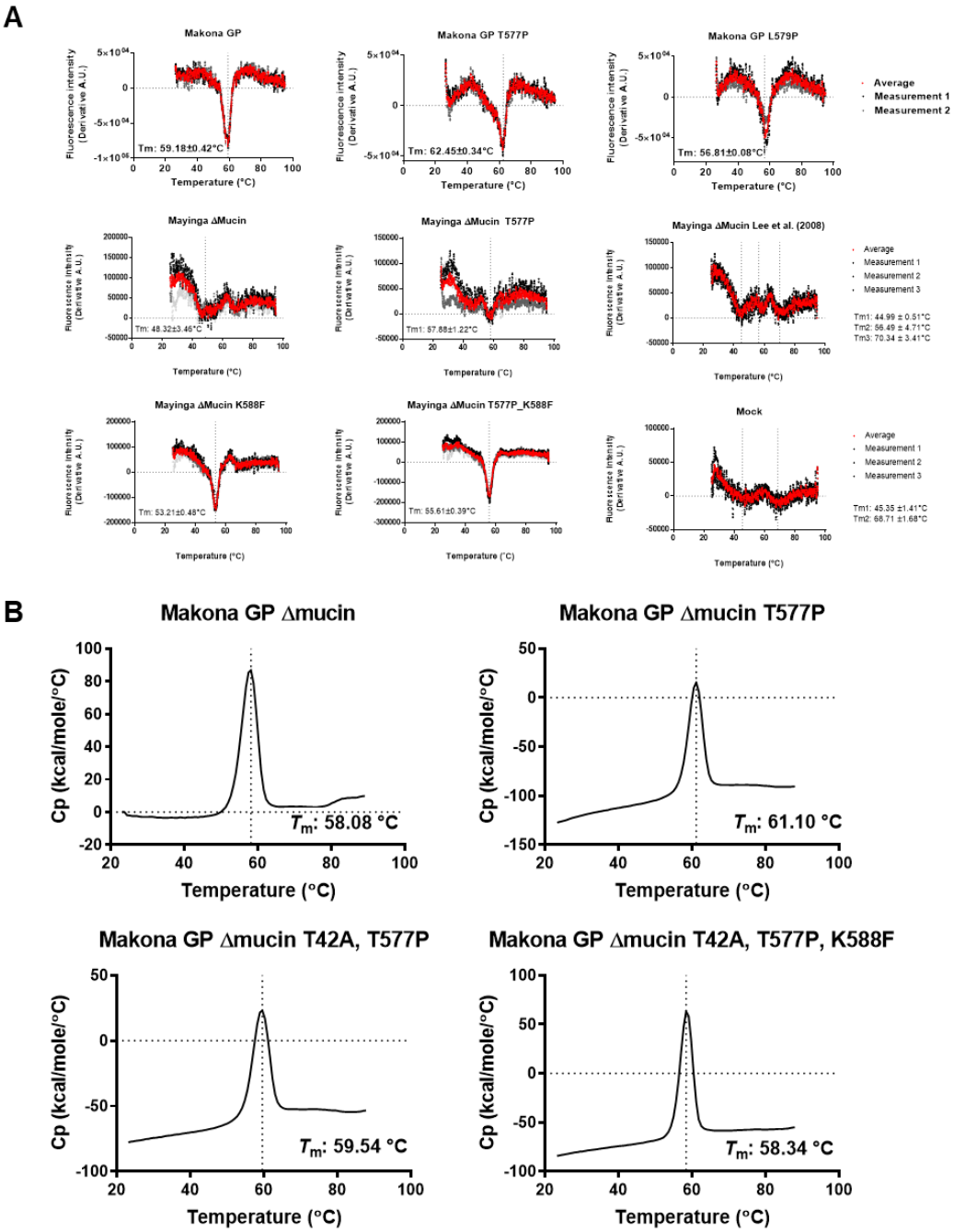

Figure S2. Temperature stability testing, Related to Figure 4A. **A**) Analysis of melting temperature (T_m) using differential scanning fluorimetry of purified Makona GP and a variant with the T577P substitution. The first order derivatives are plotted. Duplicate runs were averaged and T_m determined as the lowest derivative value representing the $T_{m\ 50}$ value. **B**) Analysis of T_m using differential scanning calorimetry of purified Makona GP Δmucin and variants with a combination of T577P, T42A and/or K588F substitutions. The specific heat capacity values are plotted and the T_m determined as the highest value.

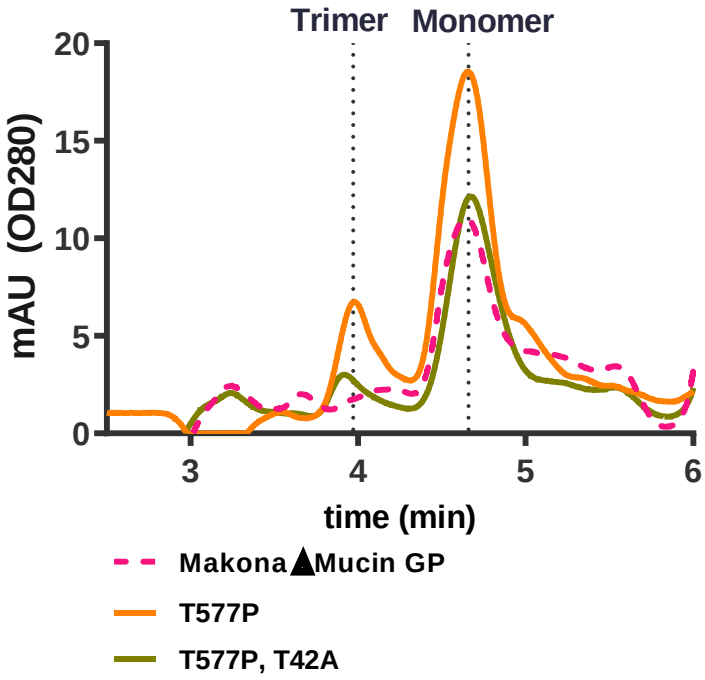

Figure S3. **Analytical SEC profile of the T577P and T42A variants of Makona ΔMucin GP,** Related to Figure 2 and 5A. Analysis was performed on crude cell culture supernatant. T42A was introduced to remove a glycan at position 40 to optimize crystallization.

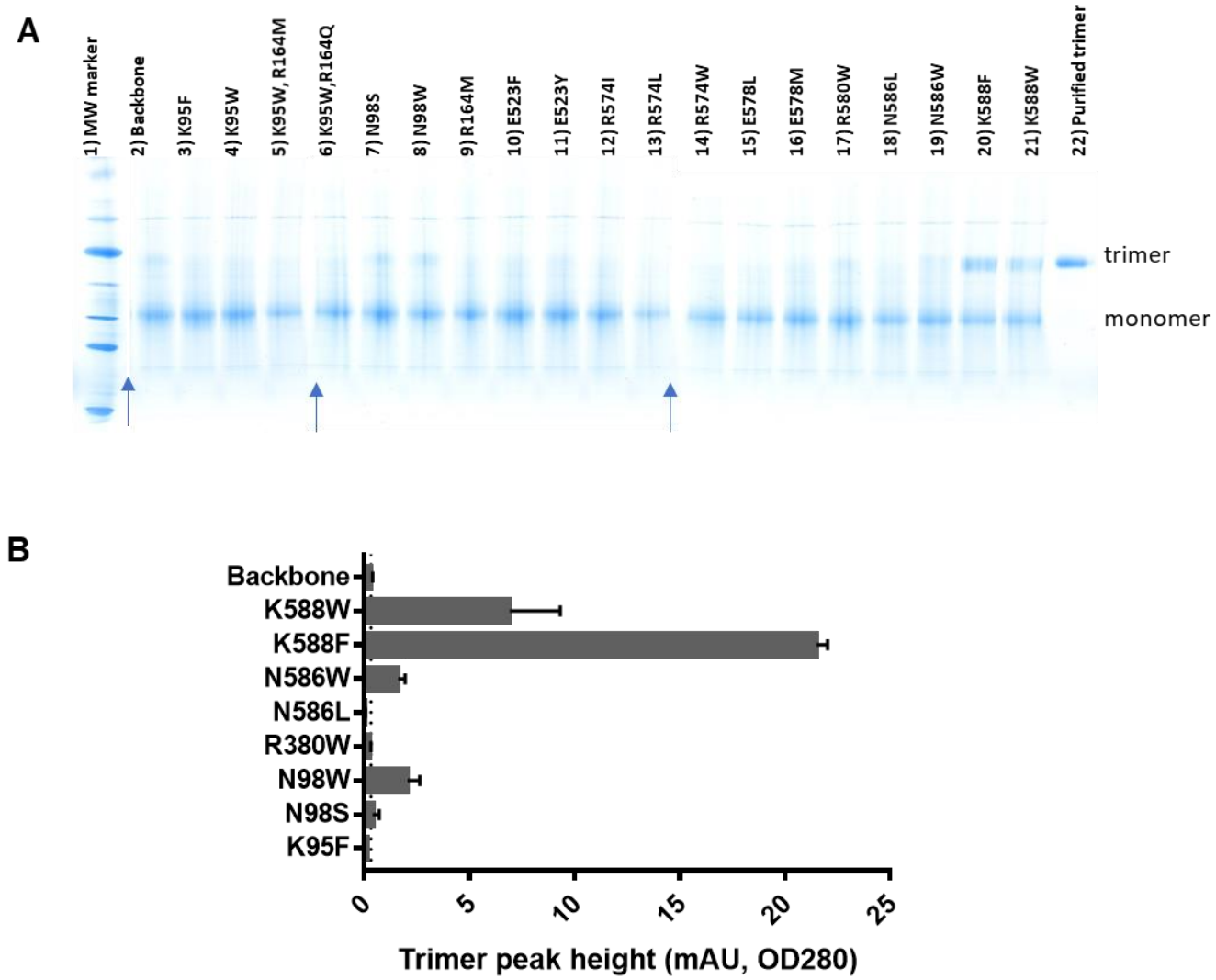

Figure S4. Native PAGE of additional substitutions introduced in the Makona ΔMucin GP T577P/T42A backbone and analytical SEC of a subset of the variants, related to Figure 3. T42A was introduced to remove a glycan site at position 40 to facilitate crystallization of the protein **A**) GP trimer levels using native PAGE with the variants in supernatant (lanes 2-21) and purified trimer (lane 22). The arrows indicate where different gels are pasted together. **B**) The trimer peak height as depicted as absorption at 280 nm in analytical SEC at 3.9 minutes (see Fig. 3A). Data are represented as mean ± SEM.

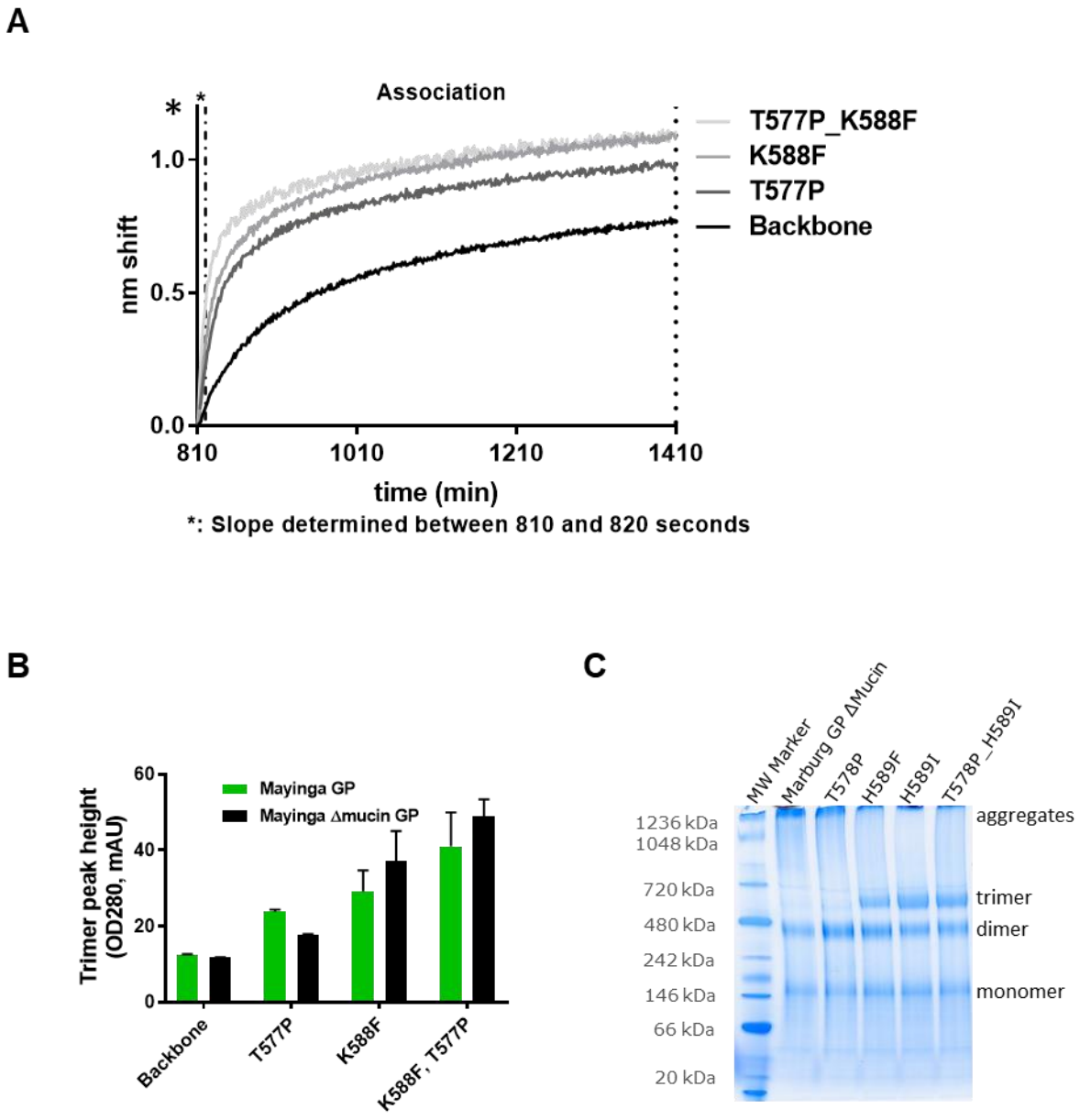

Suppl. Fig 5. Determination of trimer formation of Mayinga GPs with T577P and K588F substitutions and Marburg GP with K589F/I substitutions, related to figure 4B and C **A**) Bio-Layer Interferometry curves of Mayinga GP. The slope was determined between 810 and 820 seconds as indicated by the asterisk. Values are plotted in a bar graph in Figure 3b. **B**) Expression levels of GP trimers based on analytical SEC trimer peak heights (see Figure 4A). Data are represented as mean ± SEM. **C**) Native PAGE with crude cell culture supernatants of Marburg Δmucin GP with various substitutions labeled in the top row. The running heights of aggregates, trimers, dimers and monomers are indicated.

Table S1. SEC-MALS analysis of stabilized Marburg and Mayinga ΔMucin GPs. Related to figure 4D.

	Marburg H589F	**Marburg H589I**	**Mayinga T577P, K588F**
UV OD280 Absorption coefficient	1.012	1.028	1.566
Calulated MALS MW (kDa)	213.7±0.48	214.0±0.13	183.8±1.52
Calculated MW (kDa) based on protein sequence	173.1	166.6	155.4
Protein fraction (kDa) in MALS signal	165.2±0.44	163.2±0.60	159.3±1.70
Glycosylation fraction (kDa) in MALS signal	48.87±0.84	65.61±90	37.68±2.10
Rh (nm)	7.87±0.16	7.70±0.16	6.17±0.15

Table S2. Crystallographic data collection and refinement statistics. Related to figure 5B.

	Makona GP ΔMucin T42A/T577P/K588F
PDB ID	TBD
Data collection	
Space group	*H*32
Cell dimensions	
a, *b*, *c* (Å)	113.1, 113.1, 393.2
α, β, γ (°)	90, 90, 120
Wavelength (Å)	0.9792
Resolution (Å)	47.5–3.5 (3.83–3.50)
Unique reflections	10,491 (2,527)
R_{merge}	0.346 (0.743)
R_{pim}	0.177 (0.378)
$I / \sigma I$	3.4 (2.0)
$CC_{1/2}$	0.913 (0.564)
Completeness (%)	84.7 (86.7)
Redundancy	4.3 (4.3)
Wilson *B*-factors (Å^2)	55.3
Refinement	
Resolution (Å)	47.5–3.5 (3.85–3.50)
Unique reflections	10,491 (2,640)
R_{work} / R_{free} (%)	28.4/30.3
No. atoms	
Protein	2,773
Ligand (NAG)	42
B-factors (Å^2)	
Protein	62.1
Ligand (NAG)	64.8
R.m.s. deviations	
Bond lengths (Å)	0.008
Bond angles (°)	0.80
Ramachandran	
Favored (%)	94.8
Allowed (%)	5.2
Outliers (%)	0

Table S3. Overview of crystal structures of filovirus GP prefusion trimers. Related to figure 6.

PDB code	Experimental method	resolution	Reference	Fab fragments bound or other compounds	N-terminal extended	Trimerization domains	Virus	Last visible residue	pH	Space group
3CSY	X-ray	3.40	Lee et al.	KZ52 Fab	Yes	**No**	Zaire	598	8.5	*H* 3 2
3S88	X-ray	3.35	Dias et al.	16F6 Fab	Yes	**No**	Sudan	615	8.4	*I* 2 3
3VE0	X-ray	3.35	Bale et al.	16F6 Fab	Yes	**No**	Sudan	614	8.4	*I* 2 3
5F1B	X-ray	2.30	Wang et al.	receptor	Yes	**No**	Zaire	598	5.5	$P\,6_3$
5HJ3	X-ray	3.30	Bornholdt et al.	KZ52	Yes	**No**	Zaire	513	4.7	*H* 3
5FHC	X-ray	6.70	Misasi et al.	100 and 114	**No**	Yes	Zaire	599	7.5	*H* 3 2
5JNX	EM	6.56	Gong et al.	receptor	Yes	**No**	Zaire	598		NA
5JQ7	X-ray	2.69	Zhao et al.	Toremifene	Yes	Yes	Zaire	632	5.2	*H* 3 2
5JQB	X-Ray	2.68	Zhao et al.	ibuprofen	Yes	Yes	Zaire	632	5.2	*H* 3 2
5JQ3	X-ray	2.23	Zhao et al.	**no ligand**	Yes	Yes	Zaire	631	5.2	*H* 3 2
5KEL	EM	4.30	Pallesen et al.	c2G4 and c13C6	**No**	**No**	Zaire	615		NA
5KEN	EM	4.40	Pallesen et al.	c2G4 and c13C7	**No**	**No**	Zaire	615		NA
6F5U	X-ray	2.07	Ren et al.	BEPRIDIL	Yes	Yes	Zaire	632	5.2	*H* 3 2
6F6S	X-ray	2.29	Ren et al.	benztropine	Yes	Yes	Zaire	632	5.2	*H* 3 2
6F6N	X-ray	2.15	Ren et al.	sertraline	Yes	Yes	Zaire	632	5.2	*H* 3 2
6F6I	X-ray	2.40	Ren et al.	paroxetine	Yes	Yes	Zaire	632	5.2	*H* 3 2
6G95	X-ray	2.31	Zhao et al.	thioridazine	Yes	Yes	Zaire	631	5.2	*H* 3 2
6G9B	X-ray	2.26	Zhao et al.	imipramine	Yes	Yes	Zaire	631	5.2	*H* 3 2
6G9I	X-ray	2.19	Zhao et al.	clomipramine	Yes	Yes	Zaire	631	5.2	*H* 3 2
6DZM	EM	4.29	Murin et al.	ADI-15878 Fab	**No**	**No**	Bundibugyo	625		NA
6DZL	EM	4.14	Murin et al.	ADI-15878 Fab	Yes	**No**	Makona	597		NA
6EA7	X-ray	4.25	West et al.	ADI-15878 Fab	Yes	**No**	Zaire	612	7.5	$P\,3_1\,2\,1$
6EA5	X-ray	4.75	West et al.	ADI-15878 Fab	**No**	**No**	Bundibugyo	612	8.5	$P\,3_1\,2\,1$
6EAY	X-ray	3.72	Janus et al.	CA45 Fab	Yes	**No**	Zaire	614	6.0	*H* 3 2
XXXX	X-ray	3.50	This paper	**no ligand**	**No**	**No**	Makona	620	5.2	*H* 3 2